

Young's experiment with a double slit of sub-wavelength dimensions

Kanghee Lee, Jongseok Lim, and Jaewook Ahn*

Department of Physics, KAIST, Daejeon 305-701, South Korea

*jwahn@kaist.ac.kr

Abstract: We report that the interference pattern of Young's double-slit experiment changes as a function of polarization in the sub-wavelength diffraction regime. Experiments carried out with terahertz time-domain spectroscopy reveal that diffracted waves from sub-wavelength-scale slits exhibit either positive or negative phase shift with respect to Gouy phase depending on the polarization. Theoretical explanation based on the induction of electric current and magnetic dipole in the vicinity of the slits shows an excellent agreement with the experimental results.

© 2013 Optical Society of America

OCIS codes: (050.1940) Diffraction; (050.5080) Phase shift; (050.6624) Subwavelength structures; (300.6495) Spectroscopy, terahertz.

References and links

1. E. Hecht, *Optics*, 4th ed. (Addison Wesley, 2002).
2. J. D. Jackson, *Classical Electrodynamics*, 3rd ed. (Wiley, 1999).
3. F. J. García-Vidal, H. J. Lezec, T. W. Ebbesen, and L. Martín-Moreno, "Multiple paths to enhance optical transmission through a single subwavelength slit," *Phys. Rev. Lett.* **90**, 213901 (2003).
4. C. Wang, C. Du, and X. Luo, "Refining the model of light diffraction from a subwavelength slit surrounded by grooves on a metallic film," *Phys. Rev. B* **74**, 245403 (2006).
5. Y. Takakura, "Optical resonance in a narrow slit in a thick metallic screen," *Phys. Rev. Lett.* **86**, 5601 (2001).
6. F. Yang and J. R. Sambles, "Resonant transmission of microwaves through a narrow metallic slit," *Phys. Rev. Lett.* **89**, 063901 (2002).
7. M. A. Seo, H. R. Park, S. M. Koo, D. J. Park, J. H. Kang, O. K. Suwal, S. S. Choi, P. C. M. Planken, G. S. Park, N. K. Park, Q. Park, and D. S. Kim, "Terahertz field enhancement by a metallic nano slit operating beyond the skin-depth limit," *Nat. Photon.* **3**, 152-156 (2009).
8. J. H. Kang, D. S. Kim, and Q. Park, "Local Capacitor Model for Plasmonic Electric Field Enhancement," *Phys. Rev. Lett.* **102**, 093906 (2009).
9. E. H. Khoo, E. P. Li, and K. B. Crozier, "Plasmonic wave plate based on subwavelength nanoslits," *Opt. Lett.* **36**, 2498-2500 (2011).
10. P. F. Chimento, N. V. Kuzmin, J. Bosman, P. F. A. Alkemade, G. W.'t Hooft, and E. R. Eliel, "A subwavelength slit as a quarter-wave retarder," *Opt. Express* **19**, 24219-24227 (2011).
11. H. A. Bethe, "Theory of diffraction by small holes," *Phys. Rev.* **66**, 163-182 (1944).
12. M. Yi, K. Lee, J. D. Song, and J. Ahn, "Terahertz phase microscopy in the sub-wavelength regime," *Appl. Phys. Lett.* **100**, 161110 (2012).
13. K. Lee, M. Yi, S. E. Park, and J. Ahn, "Phase-shift anomaly caused by subwavelength-scale metal slit or aperture diffraction," *Opt. Lett.* **38**, 166-168 (2013).
14. D. Grischkowsky, S. Keiding, M. van Exter, and Ch. Fattinger, "Far-infrared time-domain spectroscopy with terahertz beams of dielectrics and semiconductors," *J. Opt. Soc. Am. B* **7**, 2006-2015 (1990).
15. Y.-S. Lee, *Principles of Terahertz Science and Technology* (Springer, 2009).
16. P. C. M. Planken, H.-K. Nienhuys, H. J. Bakker, and T. Wenckebach, "Measurement and calculation of the orientation dependence of terahertz pulse detection in ZnTe," *J. Opt. Soc. Am. B* **18**, 313-317 (2001).
17. Y. Kim, M. Yi, B. G. Kim, and J. Ahn, "Investigation of THz birefringence measurement and calculation in Al₂O₃ and LiNbO₃," *Appl. Opt.* **50**, 2906-2910 (2011).
18. L. G. Gouy, "Sur une propriete nouvelle des ondes lumineuses," *C. R. Acad. Sci. Paris* **110**, 1251-1253 (1890).

19. A. Rubinowicz, "On the anomalous propagation of phase in the focus," *Phys. Rev.* **54**, 931-936 (1938).
20. A. E. Siegman, *Lasers* (University Science Books, 1986).
21. A. B. Ruffin, J. V. Rudd, J. F. Whitaker, S. Feng, and H. G. Winful, "Direct observation of the Gouy phase shift with single-cycle Terahertz pulses," *Phys. Rev. Lett.* **83**, 3410-3413 (1999).
22. S. Feng and H. G. Winful, "Physical origin of the Gouy phase shift," *Opt. Lett.* **26**, 485-487 (2001).
23. K. Lee, "Fourier optical phenomena and applications using ultra broadband terahertz waves," Ph. D. Thesis, KAIST (2013).

1. Introduction

Wave diffraction from an aperture is considered well understood in the context of Kirchhoff's scalar diffraction theory [1, 2]. However, when aperture size becomes equivalent to or smaller than the wavelength, vectorial nature of electromagnetic waves results in novel sub-wavelength optical phenomena [3–11]. Research in near-field optical applications and subwavelength-resolution imaging exploits the dynamical interplay between the cavity field and induced edge currents, leading to observations of unprecedented phenomena including extraordinary power transmission in groove-patterned slits [3, 4], Fabry-Perot-like thick-slit transmission [5, 6], and strong field enhancement in sub-wavelength slits [9, 10]. Our previous study considered the diffraction phase of sub-wavelength-scale apertures and slits, in which the size-dependent phase shifts were caused by induced electric currents and effective magnetic dipoles in the sub-wavelength regime [12, 13].

In this paper, we study the polarization dependence of the sub-wavelength diffraction phase and its consequence on Young's double-slit interference patterns. For this, we consider terahertz (THz) frequency wave diffraction from double slits with asymmetric widths. The difference of the slit-width dependent diffraction phase shifts results in spatial shift of the interference patterns. Furthermore, as the diffraction phase is strongly coupled with the polarization state of the incident wave, the diffraction pattern shows polarization-dependent behavior.

2. Young's double-slit interference pattern in the sub-wavelength regime

Let us consider wave diffraction from asymmetric double slits with respectively width d_1 and d_2 ($d_1 < d_2$) and with spacing a , as shown in Fig. 1. When electromagnetic wave of angular frequency ω diffracts from the slits and we assume that $D_{1,2}$ and $\phi_{1,2}$ are respectively the amplitude and phase of the transmitted wave from each slit, the electric field sum in the far-field diffraction region is given by

$$E(x, \omega) = \int \left(D_1 e^{i\phi_1} \delta(x' + \frac{a}{2}) + D_2 e^{i\phi_2} \delta(x' - \frac{a}{2}) \right) e^{i\frac{kx'}{f}} dx', \quad (1)$$

where $\delta(x)$ is Dirac delta function, f is the focal length of the imaging lens, and k is the wave number. Note that $D_{1,2}$ could not just be proportional to $d_{1,2}$ and $\phi_{1,2}$ could be different from 90 degree Gouy phase shift, in the sub-wavelength regime [13]. The resulting interference pattern is given by

$$I(x, \omega) = |E(x, \omega)|^2 = 4D_1 D_2 \cos^2 \left(\frac{ka}{2f} x - \frac{\Delta\phi}{2} \right) + (D_2 - D_1)^2, \quad (2)$$

where the diffraction phase difference, $\Delta\phi = \phi_2 - \phi_1$, is given as a function of d_1 and d_2 . So, for a non-zero $\Delta\phi$ the interference pattern is not given symmetrical to the optical axis, different from what is expected from Kirchhoff's scalar diffraction theory. Furthermore, $\Delta\phi$ is also strongly coupled with the polarization angle θ (to be explained in Sec. 4). So, it is expected that the location of the interference pattern changes as a function of θ , in the sub-wavelength regime.

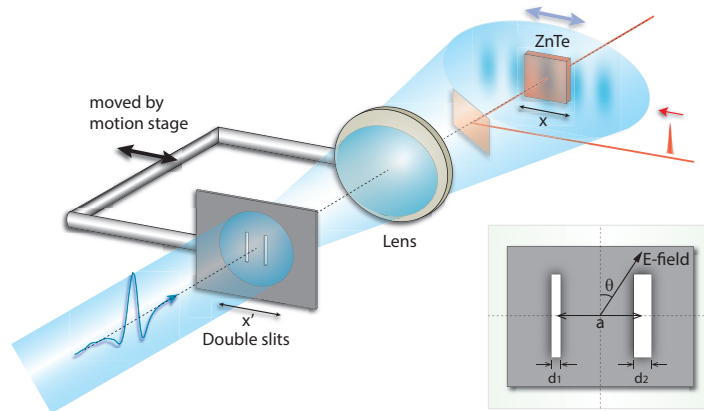


Fig. 1. Experimental setup to measure sub-wavelength Young's double-slit diffraction pattern. Inset shows double-slit geometry and electric field polarization angle.

In the remaining sections, experimental verification of the double-slit interference patterns in the sub-wavelength regime is given as following: we first briefly describe the experiments in Sec. 3. Then, we study the polarization dependence of the diffraction phase and amplitude from single slits of sub-wavelength sizes in Sec. 4. Based on these results, we return to discuss the results of Young's double-slit experiments in the sub-wavelength diffraction regime in Sec. 5, before we conclude in Sec. 6.

3. Experimental description

Experiments were performed with a transmission-type THz time-domain spectroscopy (THz-TDS) setup. THz pulses were generated from a conventional photoconductive antenna irradiated with femtosecond near-infrared laser pulses from a Ti:sapphire mode-locked laser oscillator [14, 15]. The THz pulses were then measured via laser-gated electro-optical sampling with a 2-mm-thick $\langle 110 \rangle$ -oriented ZnTe crystal and their time-domain waveforms were recorded as a function of time delay between the THz pulse generation and detection. Note that both the THz generation and detection are polarization sensitive [16, 17], hence the given experiment is equivalent to a slit rotation within a pair of parallel linear polarizers. For the single-slit experiments to be explained in Sec. 4, we used commercial single slits made out of freestanding stainless steel with a thickness of $12.8 \mu\text{m}$, a length of $L = 3 \text{ mm}$, and various widths of 30, 40, 50, 100, 150, and $200 \mu\text{m}$, respectively. The slits were inserted at the focus of the propagating THz waves in a one-dimensional $4-f$ or $8-f$ geometry THz beam delivery system composed of two or four teflon lenses with focal length $f = 100 \text{ mm}$. For the double-slit experiments to be explained in Sec. 5, double-slits were fabricated via laser micro-machining on an aluminum sheet of thickness $18 \mu\text{m}$, and the sizes of the slits were $d_1 = 100 \mu\text{m}$ and $d_2 = 300 \mu\text{m}$, respectively, and the slit spacing was $a = 10 \text{ mm}$. Note that the incoming THz beam was collimated near the slit structure with a uniform intensity region over $20 \times 20 \text{ mm}^2$ [13]. The interference pattern was measured by moving the slits and lenses together as shown in Fig. 1 instead of the detector for convenience.

4. Polarization dependence of sub-wavelength-scale single-slit diffraction

In single-slit experiments, linearly-polarized wave of polarization angle θ with respect to the slit orientation diffracts through a slit of width d and of length L as shown in Fig. 2(a). Note

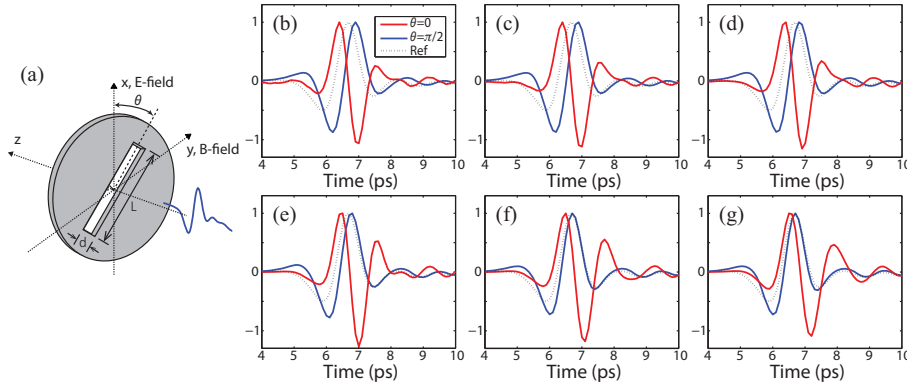


Fig. 2. (a) Experimental geometry of sub-wavelength-scale single-slit transmission. (b-g) Measured electric fields through slits of respective width of (b) $d = 30$, (c) 40, (d) 50, (e) 100, (f) 150, and (g) 200 μm . Red and Blue lines represent $\theta = 0$ and $\pi/2$, respectively. Dotted lines denotes reference fields without slits. Each signal is normalized to its maximum.

that the electric field within the slit strongly depends on θ , while the magnetic field does not, due to the symmetric boundary consideration [2, 11]. So, the physical origin of the resulting diffraction wave also changes depending on the polarization state of the incident wave.

Perpendicular polarization case ($\theta = \pi/2$): Waveguide theory predicts in this polarization case that the propagation mode of electric field exists, regardless of the size of d [2], and the electric field becomes even strongly enhanced in small d limit [7, 8]. While, the magnetic field remains the same as the incident magnetic field. The transmission wave in this geometry, therefore, comes from two distinct contributions: The first one $E_t(R)$ is the ordinary d/λ -dependent diffraction field from the scalar diffraction theory, and the second one $E_i(R)$ is the induced field from the enhanced electric field minus the incident electric field on the slit. Recent experiment shows that $E_i(R)$ has λ -dependent field enhancement compared to the first one [7] and $E_i(R)$ should be a constant of d/λ due to scale invariance [8, 13]. So, also including the phase $\pi/2$ between $E_t(R)$ and $E_i(R)$ [13], the net transmission field amplitude is obtained as

$$E_{\perp}(R) = \left(\alpha + \frac{d}{i\lambda}\right) \frac{LE_0}{R} e^{i(kR - \omega t)}, \quad (3)$$

where α is a proportional constant. Note that the phase shift compared from the phase factor, $e^{i(kR - \omega t)}$, changes from the usual $\pi/2$ advancement, or Gouy phase [18–22], to a lesser time advancement in sub-wavelength width slit, which result is given in the space domain notation as $\phi_1 > \phi_2$ in Eq. (2).

Parallel polarization case ($\theta = 0$): The electric field is negligibly small in this polarization geometry due to the boundary condition on metal, so the diffracted field is mainly contributed by the remaining magnetic field. Based on the Bethe's effective magnetic dipole model [11], one could treat this diffraction field as an effective magnetic dipole radiation. From the constant magnetic field constraint inside the slit, the effective magnetic surface charge density can be calculated. When we assume L long enough, the magnetic surface charge density $\rho(y)$ across the slit (y -direction) is given by

$$\rho(y) = -\frac{H_0}{2\pi} \frac{y}{\sqrt{\frac{d^2}{4} - y^2}}, \quad (4)$$

where H_0 is the incident magnetic field amplitude and the proportional coefficient ($1/2\pi$) can be obtained from Gauss law $\nabla \cdot \mathbf{H} = 4\pi\sigma$, where σ is the effective magnetic density [23]. The effective magnetic dipole moment then becomes $m_{\text{eff}} = -H_0 d^2 L / 16$ so that the diffracted field along the optical axis is given by

$$E_{\parallel}(R) = -\frac{k^2 d^2 L E_0}{16R} e^{i(kR - \omega t)}, \quad (5)$$

where E_0 is the incident electric field amplitude and $R = \sqrt{x^2 + y^2 + z^2}$ is the propagating vector. As a result, the diffracted electric field is given proportional to d^2/λ^2 contrary to the linear d/λ -dependence expected in the scalar diffraction theory. So, the diffracted field from the slit is much smaller than what is expected from Kirchhoff's diffraction theory in the small d limit. Note that this d/λ -ratio reduction from Kirchhoff's theory is similar to the case of sub-wavelength-scale hole diffraction [11]. The phase of the diffracted electric field for $\theta = 0$ is $\pi/2$ more time-advanced than usual Gouy phase shift, so the net phase shift is π (time advancement) from $e^{i(kR - \omega t)}$. Note that both this polarization case and the sub-wavelength circular aperture case [11] are treated as effective magnetic dipole radiation [13]. For intermediate size slits, the phase advancement is between $\pi/2$ to π like sub-wavelength hole diffraction due to the optical theorem [13]. Therefore, the phase shift changes oppositely from the $\theta = \pi/2$ case, or $\phi_1 < \phi_2$ in the notation of Eq. (2).

Diffraction phase: The phase shifts of the diffracted waves from sub-wavelength-scale slits were directly measured in our THz waveform detection. Figures 2(b)-2(g) represent the normalized time-signals of the diffracted THz waves from 30, 40, 50, 100, 150, and 200 μm slits, respectively. The blue and red lines in Fig. 2 represent $\theta = 0$ and $\theta = \pi/2$ cases, respectively, while the reference signals without a slit are plotted in dotted lines. Phase advancement and retardation of nearly $\pi/2$ are clearly observed in 30 μm -slit diffraction shown in Fig. 2(b) so the fields in $\theta = \pi/2$ and $\theta = 0$ have opposite phases to each other. For intermediate size, phase difference between $\theta = \pi/2$ and $\theta = 0$ becomes smaller as shown in Figs. 2(c)-2(g).

Diffraction amplitude: The amplitudes of the diffracted waves from sub-wavelength-scale slits are shown in Fig. 3, where the measured fields through sub-wavelength-scale slits for $\theta = \pi/2$ and $\theta = 0$ are respectively in Figs. 3(a) and 3(c). The scaling behaviors of the diffracted wave amplitude in Eqs. (3) and (5) are verified respectively in Fig. 3(b) for $\theta = \pi/2$ and in Fig. 3(d) for $\theta = 0$. As expected, significant amount of fields are transmitted for $\theta = \pi/2$ even in the smallest slit of $d = 30 \mu\text{m}$, while negligible amount transmitted for $\theta = 0$. Note that the d^2/λ^2 dependence of the transmission amplitude for $\theta = 0$ in Fig. 3(d) breaks off from the cutoff wavelength condition at $d/\lambda = 0.5$ in waveguide theories [2].

The phase and amplitude behaviors of diffracted waves from sub-wavelength-scale single slits can be summarized in Table 1, where the large slit case is based on Kirchhoff's diffraction theory.

Table 1. Phase and amplitude behaviors of sub-wavelength-scale slit diffraction

	Small slit limit		Large slit (Kirchhoff)
	$\theta = \pi/2$	$\theta = 0$	$d \gg \lambda$
phase	0	π	$\pi/2$ (Gouy phase)
amplitude	no dependence	quadratic (d^2/λ^2)	linear (d/λ)

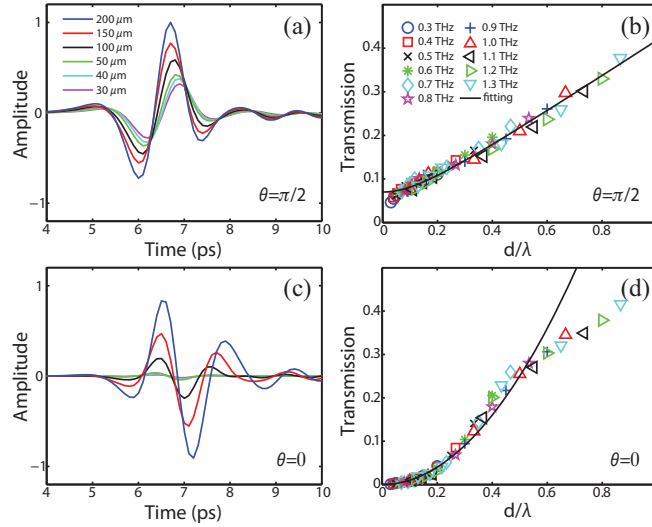


Fig. 3. Transmitted THz waves through sub-wavelength-scale single slits. (a) Measured time signals in $\theta = \pi/2$ case and (b) their relative transmission amplitude (divided by reference signals without slits) plotted as a function of d/λ . (c) Measured time signals in $\theta = 0$ case and (d) their relative transmission amplitude plotted as a function of d/λ . Black lines in (b) and (d) represent fitting lines based on Eqs. (3) and (5), respectively. (a) and (c) are plotted in the same scale.

5. Results of double-slit interference pattern in the sub-wavelength regime

Figures 4 (a)-4(c) show the experimental results of double-slit interference pattern in the sub-wavelength regime for perpendicularly polarized waves ($\theta = \pi/2$). The measured THz time signal $E_{\perp}(x, t)$, the interference pattern spectrum $I(x, \omega)$, and the interference pattern $I(x, \omega_0)$ at $\omega_0 = 0.7$ THz are shown in Figs. 4(a)-4(c), respectively. In this polarization, the interference pattern is shifted to the direction of the first (narrow) slit, because the transmitted field from the first slit has time retardation compared to the second (wide) slit (*i.e.*, $\phi_1 > \phi_2$) as shown in Figs. 4(b) and 4(c). Based on the measurement in Sec. 4, the diffraction phase difference $\Delta\phi = \phi_2 - \phi_1 \approx -30^\circ$, which is consistent with the experimental result in Fig. 4(c). The maximum time peak also shifts to the narrow-slit direction in Fig. 4(a). The visibility of the pattern is given from Eq. (2) by

$$\frac{I_{\max} - I_{\min}}{I_{\max} + I_{\min}} = \frac{2D_1D_2}{D_1^2 + D_2^2}, \quad (6)$$

where I_{\max} and I_{\min} are the maximum and minimum of the intensity, respectively. In Kirchhoff's theory, it is given simply by $2d_1d_2/(d_1^2 + d_2^2)$ but in the sub-wavelength regime, the visibility also depends on the polarization. As found in Table 1. D_1 should be larger than what is expected from Kirchhoff's theory for the perpendicular polarized wave. So, the interference pattern should show clearer visibility in this case, which is verified in Fig. 4(c) where the experimental data (crosses) exhibits a better visibility than Kirchhoff's theory line (dash-dot).

Results for the parallel polarization case ($\theta = 0$) are shown in Figs. 4(d)-4(f). In this field polarization, the diffraction pattern is shifted to the direction of the second (wide) slit as shown in Figs. 4(e) and 4(f), which can be easily understood because the diffracted field from the narrow slit has phase advancement compared to the wide slit (*i.e.*, $\phi_1 < \phi_2$). Based on the

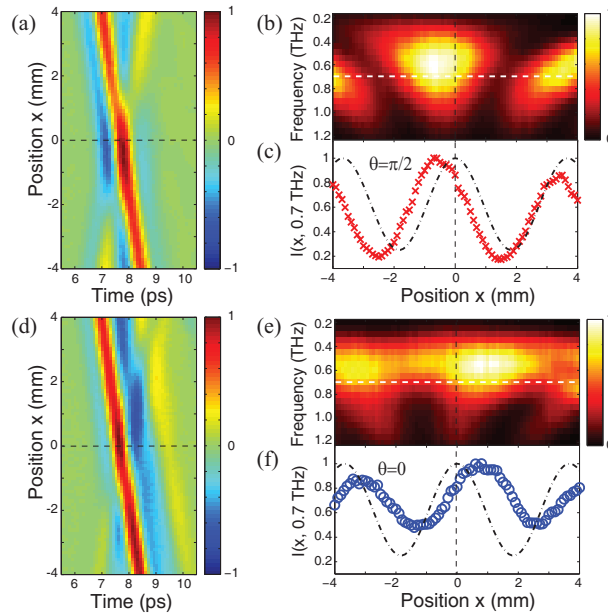


Fig. 4. Measured time signals and interference patterns. (a) Measured THz time signals in $\theta = \pi/2$ case (normalized to the max), and (b,c) corresponding interference patterns of all THz frequencies in (b) and at 0.7 THz in (c). (d) Measured THz time signals in $\theta = 0$ case (normalized to the max), and (e,f) corresponding interference patterns of all THz frequencies in (e) and at 0.7 THz in (f). All the time signals and patterns are normalized. Red crosses in (c) and Blue circles in (f) represent experimental data and Black dash-dot lines in (c,f) represent theoretical expectation based on scalar diffraction theory. White dash lines in (b) and (e) indicate 0.7 THz. Black dash lines represent the optical axis.

measurement in Sec. 4, $\Delta\phi \approx 60^\circ$. The maximum time peak also appears near the wide slit in Fig. 4(d). In addition, the experimental data (circles) exhibits poorer visibility than Kirchhoff's theory line (dash-dot) in Fig. 4(f), which can be also understood from Table 1 that D_1 in $\theta = 0$ is smaller than what is expected from Kirchhoff's theory.

6. Conclusion

In summary, we have considered asymmetric double-slit diffraction problem in the sub-wavelength regime. Experimental results show that both the location and visibility of the interference pattern are different from what are expected from Kirchhoff's scalar diffraction theory and given strongly polarization-dependent. The physical origin of this behavior is based on the polarization dependence of sub-wavelength single-slit diffraction phenomena, which can be summarized as (1) the diffraction phase shift is positive (negative) and (2) the diffraction amplitude scales quadratically (does not scale) with respect to the sub-wavelength slit width for parallel (perpendicular) polarized wave. Experimentally verified interference patterns show excellent agreement with the predictions.

Acknowledgments

This research was supported in part by Basic Science Research Programs [2013R1A2A2A05005187, 2009-0093428] and in part by the WCI Program [WCI 2011-001] through the National Research Foundation of Korea.